The Laval-Jeffcott Rotor Model 3

3.1 The Two-Degrees-of-Freedom Rotor System

The fundamental dynamic characteristics of a rotor system can be studied and analyzed by using simple rotor models. Two types of rotor models are discussed in this chapter: one is the flexible rotor with rigid bearings and the other is the rigid rotor with flexible bearings. Two-degrees-of-freedom (2 DOF) systems are considered in these models and many assumptions made here are not practical and do not correspond with reality, but they can simplify the solution and allow for parametric studies be performed. This allows us to understand the effects of each parameter on rotor dynamics behaviors. They also provide many valuable physical insights into more complicated systems.

3.1.1 The Flexible Rotor with Rigid Bearings

A single disk centrally mounted on a uniform, flexible, and massless shaft, which is supported by two identical bearings, as illustrated in Figure 3.1-1, is most widely utilized by researchers to study and understand basic rotordynamics phenomena. If the bearings are infinitely stiff (rigid bearings), this model is normally referred to as the *Laval Rotor* in Europe, and *Jeffcott Rotor* in other parts of the world.

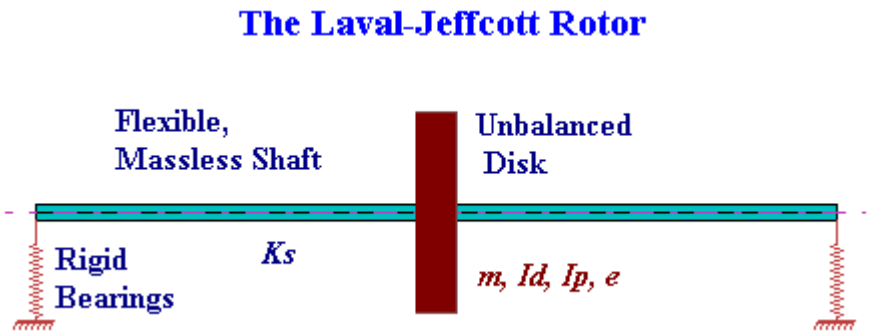

Figure 3.1-1 A simple Laval-Jeffcott rotor

For the centrally mounted disk, the system is symmetric and the first two fundamental translational and rotational motions are decoupled and can be considered separately, as

shown in Figure 3.1-2. For the pure translational motion, as shown in Figure 3.1-2 (a), the disk has maximum translational displacement and zero rotation (slope). For the pure rotational motion, as shown in Figure 3.1-2 (b), the disk has maximum rotation (slope) and zero translational displacement.

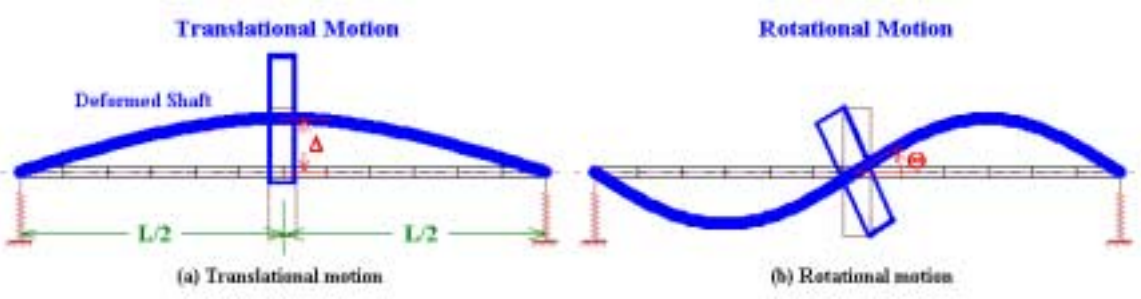

Figure 3.1-2 Two fundamental motions for a symmetric flexible rotor

Since the translational and rotational motions are decoupled, the translational and rotational stiffness of the elastic shaft can be obtained from the basic beam deflection equations. For the determination of translational shaft bending stiffness, consider a simply supported beam with a concentrated load at midspan (disk location). At midspan, the slope is zero and the defection due to the point load (F) is:

$$\Delta = \frac{FL^3}{48EI} \tag{3.1-1}$$

From the linear force-displacement relationship, the shaft bending stiffness for the fundamental translational motion is:

$$k_T = \frac{48EI}{L^3} \tag{3.1-2}$$

For the determination of rotational shaft bending stiffness, consider a simply supported beam with a moment load at midspan (disk location). At midspan, the deflection is zero and the slope due to the moment (M) load is:

$$\Theta = \frac{ML}{12EI} \tag{3.1-3}$$

Again, the shaft rotation stiffness for the fundamental rotational motion is:

$$k_R = \frac{12EI}{L} \tag{3.1-4}$$

For the Laval-Jeffcott rotor system, with flexible rotor and rigid bearings, the translational and rotational motions correspond to the first and second bending modes.

3.1.2 The Rigid Rotor with Flexible Bearings

Another simple rotor model, commonly used to study the fundamental rotordynamics, is a symmetric rigid rotor on two identical flexible supports, as illustrated in Figure 3.1-3. The rotor is considered rigid and symmetric. Again, the translational and rotational motions at the center of mass are decoupled and can be studied separately, as shown in Figure 3.1-4.

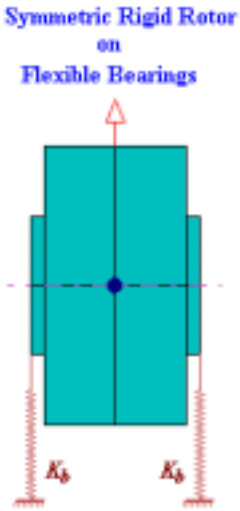

Figure 3.1-3 A symmetric rigid rotor with flexible bearings

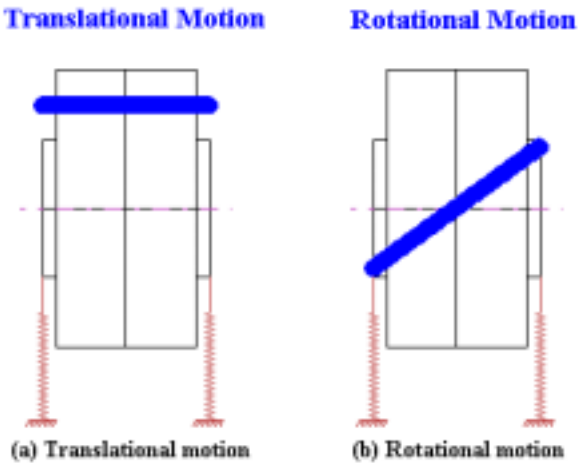

Figure 3.1-4 Two fundamental motions for a symmetric rigid rotor

Since the rotor is rigid and symmetric, and the two bearings are identical with a stiffness of K_b, the translational and rotational stiffnesses can be determined from the force and moment equations as:

$$k_T = 2k_b \qquad \text{Translational stiffness} \tag{3.1-5}$$

$$k_R = \frac{1}{2}k_b L^2 \qquad \text{Rotational stiffness} \tag{3.1-6}$$

For the symmetric rigid rotor with flexible bearings, the translational and rotational motions are commonly referred as two fundamental *rigid body modes*, i.e. *translatory* and *conical* modes.

3.2 Translational Motion

For a pure translational motion, consider a more generalized Laval-Jeffcott rotor system with flexible supports, as illustrated in Figure 3.2-1. When the bearings are flexible and each bearing has a stiffness of K_b, the equivalent stiffness of the system K, combining shaft stiffness K_s and bearing stiffness K_b is:

$$\frac{1}{K}=\frac{1}{K_s}+\frac{1}{2K_b} \quad \Rightarrow \quad K=\frac{2K_bK_s}{2K_b+K_s}=\frac{K_s}{1+\dfrac{K_s}{2K_b}}=\frac{2K_b}{\dfrac{2K_b}{K_s}+1} \tag{3.2-1}$$

It is evident from Eq. (3.2-1) that when the bearing stiffness is much larger than the shaft bending stiffness ($K_b >> K_s$), the equivalent stiffness reduces to be K_s. This is a typical Laval-Jeffcott rotor system with elastic shaft and rigid supports. When the shaft bending stiffness is much larger than the bearing stiffness ($K_s >> K_b$), the equivalent stiffness reduces to be $2K_b$ and it becomes a symmetric rigid rotor supported by flexible bearings.

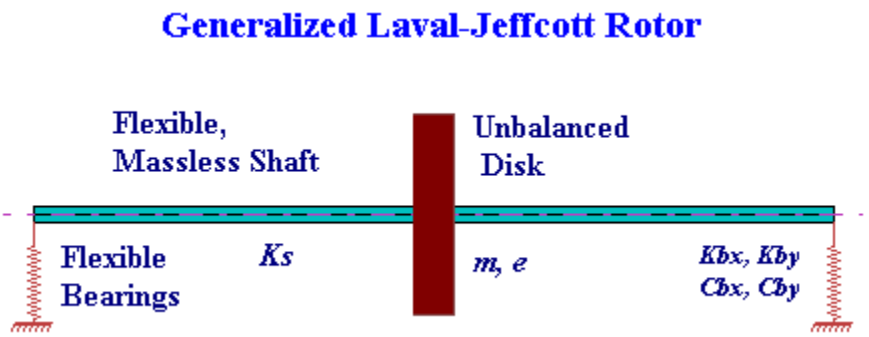

Figure 3.2-1 A generalized Laval-Jeffcott rotor

When the stiffnesses and dampings in both X and Y directions are the same, the system is referred to as an *isotropic system*. In general, the equivalent stiffnesses (K_x, K_y) and viscous dampings (C_x, C_y) in both X and Y directions, are not the same due to the asymmetric properties of the bearings, even though the shaft is axisymmetric (isotropic). This system is thus referred to as *anisotropic system*.

Consider a generalized Laval-Jeffcott rotor system with equivalent support stiffnesses of K_x and K_y and associated viscous damping C_x and C_y in the X and Y direction, as illustrated in Figure 3.2-2. The disk has a mass of m and the center of gravity is offset from the shaft geometric center by an eccentricity of e. The motion at the disk center is described by two translational displacements (x, y), as illustrated in Figure 3.2-2.

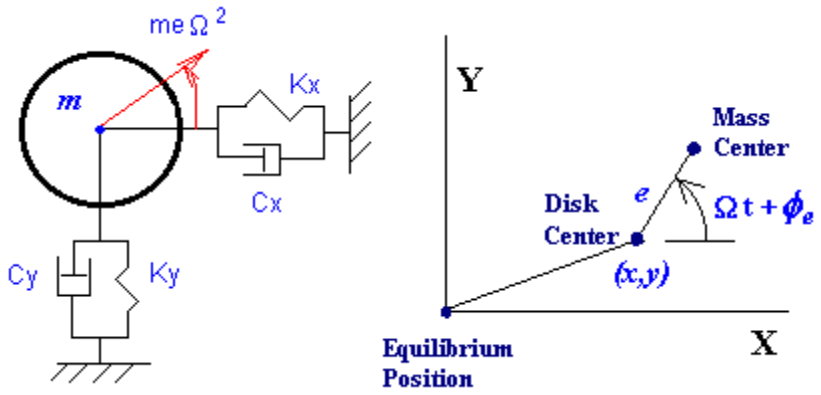

Figure 3.2-2 A two-degrees-of-freedom model

For the case of constant angular speed of rotation, Ω, the equations of motion for the mass center, can be derived from Newton's Laws of motion:

$$m\frac{d^2}{dt^2}\left(x + e\cos(\Omega t + \phi_e)\right) = -C_x\dot{x} - K_x x \tag{3.2-2}$$

$$m\frac{d^2}{dt^2}\left(y + e\sin(\Omega t + \phi_e)\right) = -C_y\dot{y} - K_y y \tag{3.2-3}$$

It can be rewritten as

$$m\ddot{x} + C_x\dot{x} + K_x x = me\Omega^2\cos(\Omega t + \phi_e) \tag{3.2-4}$$

$$m\ddot{y} + C_y\dot{y} + K_y y = me\Omega^2\sin(\Omega t + \phi_e) \tag{3.2-5}$$

where ϕ_e is the phase angle for the mass unbalance position. For single unbalance force, as in this case, ϕ_e can be set to zero without loss of generality. The equations of motion show that the motions in the X and Y directions are both dynamically (inertially) and statically (elastically) decoupled in this simple model. Therefore, they can be solved separately. Since there are no cross-coupling stiffnesses in this model, it is sometimes referred to as an *orthotropic system*. For the isotropic systems, the equations of motion for the *x* and *y* displacements are identical, except for the 90 degrees phase difference in unbalance excitations.

3.3 Natural Frequencies and Natural Modes

The undamped natural frequency, viscous damping factor (ratio), and damped natural frequency for each direction are:

$$\begin{aligned} \omega_{nx} &= \sqrt{\frac{K_x}{m}}, \qquad \zeta_x = \frac{C_x}{2m\omega_{nx}}, \qquad \omega_x = \omega_{nx}\sqrt{1-\zeta_x^2} \\ \omega_{ny} &= \sqrt{\frac{K_y}{m}}, \qquad \zeta_y = \frac{C_y}{2m\omega_{ny}}, \qquad \omega_y = \omega_{ny}\sqrt{1-\zeta_y^2} \end{aligned} \tag{3.3-1}$$

For this simple rotor system with purely translational motion, the natural frequencies are independent of the rotor spin-speed. In rotordynamics, the natural frequencies are commonly referred to as the *whirl speeds*. For each natural frequency (eigenvalue), there is an associated modal orbit (eigenvector). Since the motions in both directions are decoupled, the modal orbit at each natural frequency degenerates into a straight line. Hence, the modal orbits (eigenvectors) for the natural frequencies are:

$$\begin{aligned} &\omega = \omega_x: \quad x = |x|, \quad y = 0 \\ &\omega = \omega_y: \quad x = 0, \quad y = |x| \end{aligned} \tag{3.3-2}$$

Following the discussion from Chapter 2, the straight line path on the other hand, can be considered as being made up of two circular orbits of equal amplitude and whirling in opposite directions, with the same frequency. Therefore, each natural frequency may be treated as two natural modes with the same whirl frequency, where one is a purely forward circular mode and the other is a purely backward circular mode.

When the excitation frequency of a periodic force applied to a rotor system coincides with a natural frequency of that system, the rotor system may be in a state of *resonance* (or critical condition). The most common excitation in rotating machinery is the unbalance excitation that is synchronized with the rotor spin speed. There are other synchronous excitations, such as excitations due to shaft bow and disk skew. Non-synchronous excitations include aerodynamic excitations for compressors, gear mesh excitation for geared systems, etc. In rotating machinery, the excitation frequencies are commonly related to the rotor spin speed with a constant multiple or fraction. Traditionally, when the rotor spin speed coincides with one of the natural frequencies, the spin speed is referred to as ***critical speed***, since the unbalance excitation is the most common excitation. In a more general definition, when a rotor spin speed coincides with a constant multiple or fraction of one of the natural frequencies of the rotor system, then the spin speed is defined as a critical speed. That is, at the critical speed, one of the natural frequencies coincides with the excitation frequency.

To determine the damped critical speeds, a "*Whirl Speed Map*" is normally needed. A whirl speed map, also called "Campbell Diagram" or "Frequency Interference Diagram", is a plot of damped natural frequencies (whirl speeds) of the rotor system vs. the rotor spin speed. The damped critical speeds and any excitation resonance speeds are determined by noting the coincidence of the shaft speed with the system natural frequencies for a given excitation frequency line ($\omega_{exc} = \alpha\Omega$) in the whirl speed map. A value of one (1) in the excitation slope is associated with the synchronous excitation that is of main interest, because rotating unbalance is always present no matter how well the rotor is balanced. For the translational motion of this simple Laval-Jeffcott rotor system, the natural frequencies are independent of the spin speed. The whirl speed map with

synchronous excitation is presented in Figure 3.3-1. It shows that the first critical speed is the first natural frequency and the second critical speed is the second natural frequency in this case.

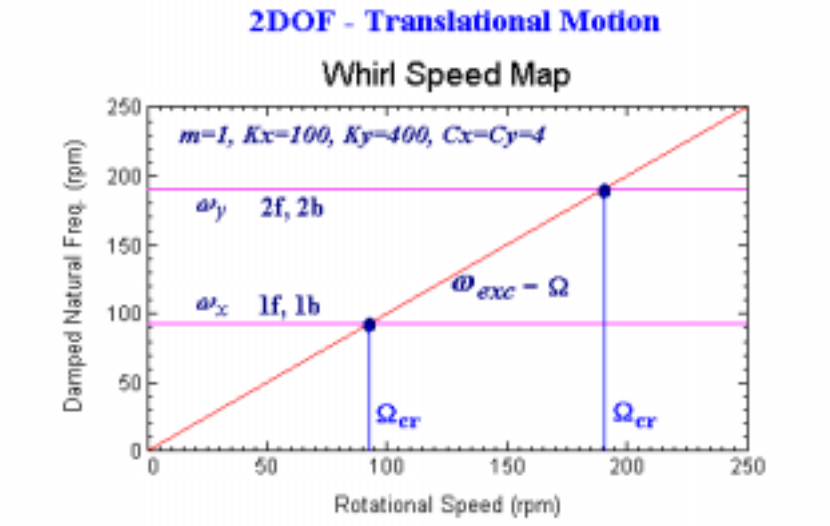

Figure 3.3-1 Whirl speed map for a 2DOF system

The modal motions at X and Y directions are decoupled in this case. There is one natural frequency for each direction of motion. Also, for each natural frequency, the associated modal orbit is a straight line in each direction. However, a straight line path can be considered as being made up of two circular orbits of equal amplitude and whirling in opposite directions, with the same natural frequency. Therefore, each natural frequency may be treated as two natural modes with the same whirl speed, where one is a purely forward (f) circular mode and the other is a purely backward (b) circular mode, as noted in Figure 3.3-1 by (1f, 1b) and (2f, 2b). Since the natural frequencies are independent of the spin speed for this simple rotor system, the natural frequencies are the critical speeds for synchronous unbalance excitation.

3.4 Steady State Response to Unbalance

Following the discussion in Chapter 1, the steady-state responses, due to mass unbalance excitation are:

$$x(t) = x_c \cos\Omega t + x_s \sin\Omega t = |x|\cos(\Omega t - \phi_x) \tag{3.4-1}$$

$$y(t) = y_c \cos\Omega t + y_s \sin\Omega t = |y|\cos(\Omega t - \phi_y) \tag{3.4-2}$$

where

$$x_c = \frac{\left(K_x - \Omega^2 m\right)\left(me\Omega^2\right)}{\left(K_x - \Omega^2 m\right)^2 + \left(\Omega C_x\right)^2}, \qquad x_s = \frac{\left(\Omega C_x\right)\left(me\Omega^2\right)}{\left(K_x - \Omega^2 m\right)^2 + \left(\Omega C_x\right)^2} \tag{3.4-3}$$

$$|x| = \frac{me\Omega^2}{\left[\left(K_x - \Omega^2 m\right)^2 + \left(\Omega C_x\right)^2\right]^{1/2}} \quad , \quad \phi_x = \arctan\left(\frac{\Omega C_x}{K_x - \Omega^2 m}\right) \tag{3.4-4}$$

and

$$y_c = \frac{\left(-\Omega C_y\right)\left(me\Omega^2\right)}{\left(K_y - \Omega^2 m\right)^2 + \left(\Omega C_y\right)^2} \ , \qquad y_s = \frac{\left(K_y - \Omega^2 m\right)\left(me\Omega^2\right)}{\left(K_y - \Omega^2 m\right)^2 + \left(\Omega C_y\right)^2} \tag{3.4-5}$$

$$|y| = \frac{me\Omega^2}{\left[\left(K_y - \Omega^2 m\right)^2 + \left(\Omega C_y\right)^2\right]^{1/2}} \quad , \quad \phi_y = \arctan\left(\frac{K_y - \Omega^2 m}{-\Omega C_y}\right) \tag{3.4-6}$$

Note that *x* and *y* displacements oscillate at the same frequency, Ω (same as rotor spin speed) with different amplitudes and phase angles. Following the discussion in Chapter 2, the steady-state unbalance response of Eqs. (3.4-1) and (3.4-2) define an elliptical motion. The ellipse properties, such as semi-major (*a*), semi-minor axes (*b*), and attitude angle (ϕ_a), may be calculated from equations given in Chapter 2. The direction of precession (whirling) of the steady state orbit, is determined by the sign of the rate of precession ($\dot{\phi}$):

$$\begin{aligned} sign\left(\dot{\phi}\right) &= sign\left(x_c y_s - x_s y_c\right) \\ &= sign\left[\left(K_x - \Omega^2 m\right)\left(K_y - \Omega^2 m\right) + \left(\Omega^2 C_x C_y\right)\right] \\ &= sign\left[\left(\omega_{nx}^2 - \Omega^2\right)\left(\omega_{ny}^2 - \Omega^2\right) + \left(\Omega^2 4\zeta_x \zeta_y \omega_{nx} \omega_{ny}\right)\right] \end{aligned} \tag{3.4-7}$$

That is,

$$\left(\omega_{nx}^2 - \Omega^2\right)\left(\omega_{ny}^2 - \Omega^2\right) + \left(\Omega^2 4\zeta_x \zeta_y \omega_{nx} \omega_{ny}\right) > 0 \quad \text{Forward Precession} \tag{3.4-8a}$$

$$\left(\omega_{nx}^2 - \Omega^2\right)\left(\omega_{ny}^2 - \Omega^2\right) + \left(\Omega^2 4\zeta_x \zeta_y \omega_{nx} \omega_{ny}\right) < 0 \quad \text{Backward Precession} \tag{3.4-8b}$$

$$\left(\omega_{nx}^2 - \Omega^2\right)\left(\omega_{ny}^2 - \Omega^2\right) + \left(\Omega^2 4\zeta_x \zeta_y \omega_{nx} \omega_{ny}\right) = 0 \quad \text{Straight Line Motion} \tag{3.4-8c}$$

From the above equations, steady-state unbalance orbit motion is a forward precession when the rotor speed is below the first resonance frequency (critical speed) and above the second resonance frequency (critical speed). The orbit motion is a backward precession between the two resonance frequencies (critical speeds) if damping does not exist. However, the backward whirl zone decreases as the damping increases, and when there is enough damping, the backward whirl does not occur at all, as illustrated in Eq. (3.4-8). Since for the isotropic systems, there is only one resonance, backward whirl does not exist. For anisotropic systems, backward whirl may exist, depending on the amount of damping present in the systems.

To gain some insights into orbit motion, an undamped orthotropic system (C_x=C_y=0) with $K_x < K_y$ is used to illustrate orbit behavior. There are two distinct resonance frequencies (critical speeds):

$$\Omega_{cr,1} = \omega_x \ < \ \Omega_{cr,2} = \omega_y \tag{3.4-9}$$

From previous equations for the steady state response, we have:

$$x_c = \frac{me\Omega^2}{K_x - \Omega^2 m} = \frac{e\Omega^2}{\omega_x^2 - \Omega^2} \quad , \quad x_s = 0 \tag{3.4-10}$$

$$y_s = \frac{me\Omega^2}{K_y - \Omega^2 m} = \frac{e\Omega^2}{\omega_y^2 - \Omega^2} \quad , \quad y_c = 0 \tag{3.4-11}$$

and

$$sign(x_c y_s - x_s y_c) = sign\left[\left(\omega_x^2 - \Omega^2\right)\left(\omega_y^2 - \Omega^2\right)\right] \tag{3.4-12}$$

Thus, the steady-state response becomes:

$$x(t) = x_c \cos\Omega t = \frac{e\Omega^2}{\omega_x^2 - \Omega^2}\cos\Omega t \tag{3.4-13}$$

$$y(t) = y_s \sin\Omega t = \frac{e\Omega^2}{\omega_y^2 - \Omega^2}\sin\Omega t \tag{3.4-14}$$

The above expressions satisfy the following relationship:

$$\left(\frac{x(t)}{x_c}\right)^2 + \left(\frac{y(t)}{y_s}\right)^2 = 1 \tag{3.4-15}$$

As expected, the above equation defines an elliptical orbit. The steady-state unbalance response for this undamped orthotropic 2DOF system is presented in Figure 3.4-1. The pertinent parameters are listed in the plot for reference. The orbit motions for various rotor speeds are analyzed and summarized below:

Case 1: $\Omega < \omega_x$ below the first critical speed

$x_c > 0, \quad y_s > 0, \quad x_c > y_s$

$a = x_c, \quad b = y_s, \quad \phi_a = 0, \quad \dot{\phi} > 0$

The motion is a forward elliptical orbit where the semi-major axis is aligned with the X axis.

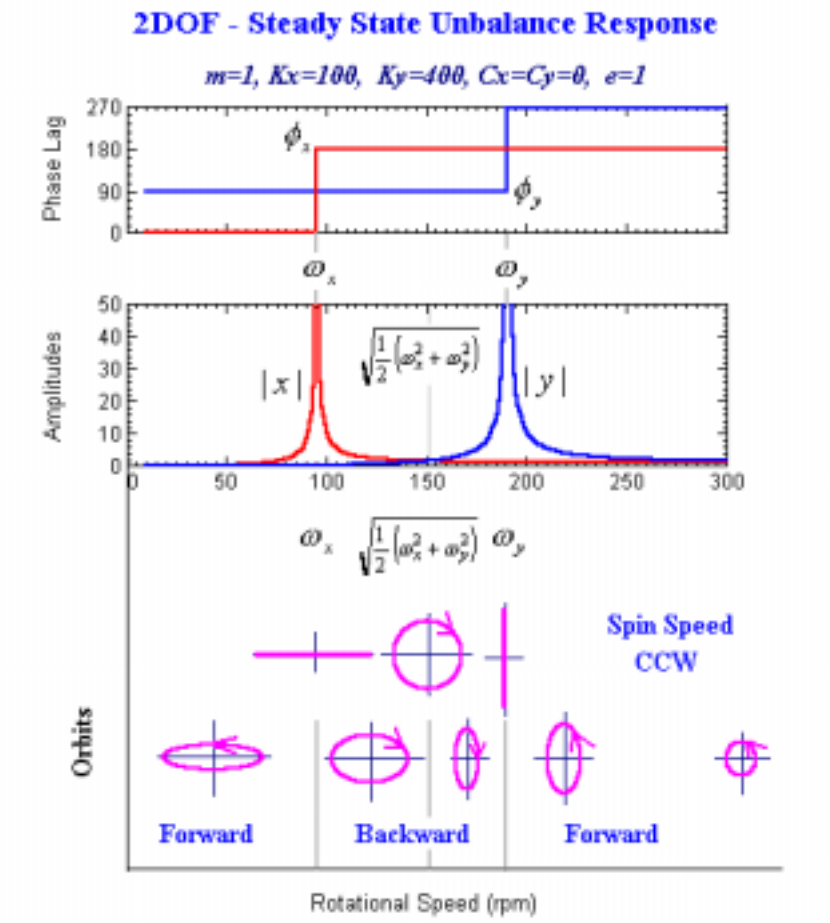

Figure 3.4-1 The steady state unbalance response and orbit analysis

Case 2: $\Omega = \omega_x$ on the first critical speed (at resonance)

$$x_c = \infty, \quad y_s > 0, \quad x_c > y_s$$
$$a = \infty, \quad b = y_s, \quad \phi_a = 0, \quad \dot{\phi} = 0$$

The motion is an unbounded straight line (resonance) aligned with the X axis. In practice, the amplitude is limited by the damping and geometric constraints.

Case 3: $\omega_x < \Omega < \sqrt{\frac{1}{2}\left(\omega_x^2 + \omega_y^2\right)}$ between the critical speeds

$$x_c < 0, \quad y_s > 0, \quad |x_c| > y_s$$
$$a = |x_c|, \quad b = -y_s, \quad \phi_a = 0, \quad \dot{\phi} < 0$$

The motion is a backward elliptical orbit where the semi-major axis is aligned with the X axis.

Case 4: $\Omega = \sqrt{\frac{1}{2}\left(\omega_x^2 + \omega_y^2\right)}$ between the critical speeds

$$x_c < 0, \quad y_s > 0, \quad |x_c| = y_s$$
$$a = |x_c|, \quad b = -a, \quad x_c = -y_s, \quad \phi_a = 0, \quad \dot{\phi} < 0$$

The motion is a purely backward **circular** orbit.

Case 5: $\sqrt{\frac{1}{2}\left(\omega_x^2 + \omega_y^2\right)} < \Omega < \omega_y$ between the critical speeds

$$x_c < 0, \quad y_s > 0, \quad |x_c| < y_s$$
$$a = y_s, \quad b = x_c, \quad \phi_a = 90, \quad \dot{\phi} < 0$$

The motion is a backward elliptical orbit where the semi-major axis is aligned with the Y axis.

Case 6: $\Omega = \omega_y$ on the second critical speed (at resonance)

$$x_c < 0, \quad y_s = \infty, \quad |x_c| < y_s$$
$$a = \infty, \quad b = x_c, \quad \phi_a = 90, \quad \dot{\phi} = 0$$

The motion is an unbounded straight line (resonance) aligned with the Y axis. In practice, the amplitude is limited by the damping and geometric constraints.

Case 7: $\Omega > \omega_y$ above the second critical speed

$$a = |y_s|, \quad b = x_c, \quad \phi_a = 90, \quad \dot{\phi} > 0$$

The motion is a forward elliptical orbit where the semi-major axis is aligned with the Y axis.

Case 8: $\Omega = \infty$ far above the second critical speed

$$a = b = |x_c| = |y_s| = e, \quad x_c = y_s = -e, \quad \phi_a = 0, \quad \dot{\phi} > 0$$

The motion is a purely forward **circular** orbit where the radius is equal to the mass eccentricity.

It is evident from Figure 3.4-1 that:

1. There are two distinct natural frequencies (critical speeds), ω_x and ω_y for X and Y directions, respectively. The motions become infinite straight lines when the rotor spin speeds are at critical speeds $(\Omega = \omega_x,\ \Omega = \omega_y)$.

2. Phase angle in the X displacement, ϕ_x, is zero before the first critical speed, ω_x, and becomes 180 degrees after the first critical speed. The phase angle changes from zero to 180 degrees at critical speed. Phase angle in the Y displacement, ϕ_y, behaves the same, except it has a 90 degrees phase lag due to the 90 degrees lag in the unbalance excitation.

3. The direction of precession can be easily identified by using the phase angle relationship when the phase angles are available:

When $\Omega < \omega_x$,	$\pi > (\phi_y - \phi_x) > 0$	Forward precession
When $\omega_x < \Omega < \omega_y$,	$\pi > (\phi_x - \phi_y) > 0$	Backward precession
When $\Omega = \omega_x,\ \Omega = \omega_y$,	$\phi_y = \phi_x$	Straight line

For the isotropic systems ($K_x = K_y$ and $C_x = C_y$), the natural frequencies are the same for both directions. From previous equations, we have:

$$\omega_n = \omega_{nx} = \omega_{ny}$$

$$x_c = y_s \quad \text{and} \quad y_c = -x_s$$

and

$$b = a \qquad \text{(circular orbit)}$$

$$sign(x_c y_s - x_s y_c) = sign(x_c^2 + y_c^2) > 0 \qquad \text{(forward whirl)}$$

Therefore, for the ***isotropic*** systems the steady-state unbalance response orbit motion is a purely ***forward circular*** whirl, with the whirl speed equal to the shaft spinning speed. That is, the steady-state unbalance response is a *forward synchronous circular motion* for the isotropic systems without any backward whirl.

Complex Notation

It is sometimes desirable and convenient to analyze the equations of motion and solutions by using complex displacements. The harmonic excitation can be represented by complex vector, and the response orbit motion can be represented by a combination of the forward and backward circular precessions of the motion. The equations of motion for a simple 2DOF Laval-Jeffcott rotor system in complex notation becomes

$$m\ddot{\hat{r}} + C_p\dot{\hat{r}} + C_m\dot{\hat{r}}^* + K_p\hat{r} + K_m\hat{r}^* = me\Omega^2 e^{j\Omega t} \tag{3.4-16}$$

where

$$\begin{aligned}\hat{r}(t) &= x(t) + j\ y(t)\\ &= \hat{r}_f e^{j\Omega t} + \hat{r}_b e^{-j\Omega t}\end{aligned} \tag{3.4-17}$$

and the complex conjugate vector is

$$\begin{aligned}\hat{r}^*(t) &= x(t) - j\ y(t)\\ &= \hat{r}_f^{\ *} e^{-j\Omega t} + \hat{r}_b^{\ *} e^{j\Omega t}\end{aligned} \tag{3.4-18}$$

also,

$$C_p = \frac{1}{2}\left(C_x + C_y\right), \qquad C_m = \frac{1}{2}\left(C_x - C_y\right) \tag{3.4-19}$$

$$K_p = \frac{1}{2}\left(K_x + K_y\right), \qquad K_m = \frac{1}{2}\left(K_x - K_y\right) \tag{3.4-20}$$

Differentiating Equations (3.4-17) and (3.4-18), and substituting into Equation (3.4-16), yields:

$$\hat{r}_f = \frac{1}{\Delta}\left(K_p - m\Omega^2 + j\Omega C_p\right) me\Omega^2 \tag{3.4-21}$$

$$\hat{r}_b^{\ *} = \frac{-1}{\Delta}\left(K_m + j\Omega C_m\right) me\Omega^2 \tag{3.4-22}$$

where

$$\Delta = \left(K_p - m\Omega^2 + j\Omega C_p\right)^2 - \left(K_m + j\Omega C_m\right)^2 \tag{3.4-23}$$

For isotropic systems, $K_m = 0, C_m = 0$, we then have $\hat{r}_b = \hat{r}_b^{\ *} = 0$. The response orbit is a purely forward circular motion.

For anisotropic undamped systems, we have:

$$\hat{r}_f = \frac{\left(\frac{1}{2}\left(\omega_x^2 + \omega_y^2\right) - \Omega^2\right) e\Omega^2}{\left(\omega_x^2 - \Omega^2\right)\left(\omega_y^2 - \Omega^2\right)} \tag{3.4-24}$$

$$\hat{r}_b = \frac{\frac{-1}{2}\left(\omega_x^2 - \omega_y^2\right) e\Omega^2}{\left(\omega_x^2 - \Omega^2\right)\left(\omega_x^2 - \Omega^2\right)} \tag{3.4-25}$$

From the above equations, the response can be divided into several spinning speed zones:

$\Omega < \omega_x$ and $\Omega > \omega_y$ $\Rightarrow |\hat{r}_f| > |\hat{r}_b|$ Forward elliptical whirl

$\omega_x < \Omega < \omega_y$ $\Rightarrow |\hat{r}_f| < |\hat{r}_b|$ Backward elliptical whirl

$\Omega = \sqrt{\frac{1}{2}\left(\omega_x^2 + \omega_y^2\right)}$ $\Rightarrow |\hat{r}_f| = 0$ Purely backward circular whirl

These conclusions are in agreement with the previous discussion.

Example 3.1: 2DOF System – Steady State Unbalance Response

Before we move on to more practical and general examples, a generalized 2DOF orthotropic system, subject to unbalance excitation, is presented in this example. The pertinent parameters are listed below:

$$m = 1,\ K_x = 100,\ K_y = 400,\ C_x = C_y = C = 4,\ e = 1$$

The equations of motion are:

$$m\ddot{x} + C_x\dot{x} + K_x x = me\Omega^2 \cos(\Omega t)$$

$$m\ddot{y} + C_y\dot{y} + K_y y = me\Omega^2 \sin(\Omega t) = me\Omega^2 \cos(\Omega t - \frac{\pi}{2})$$

There are several ways to model this simple 2DOF system in ***DyRoBeS***. Since we are going to perform some parametric studies, the simplest way to construct the rotor system is demonstrated in this example. The rotor system contains a dummy shaft element with a zero mass density and a zero elastic modulus, as shown in Figure 3.4-2. The rotational degrees-of-freedom at station 1, and all four degrees-of-freedom (translational and rotational) at station 2 are constrained. A concentrated mass with an unbalance and a bearing with translational properties, are placed at station 1. They are the only active components in this case.

Figure 3.4-2 2DOF model

Formulas for the basic parameters and results have been presented before and are listed below for reference.

$\omega_n = \sqrt{\frac{K}{m}}$ Undamped natural frequency

$\xi = \frac{C}{2m\omega_n}$ Damping factor

$\omega_d = \omega_n\sqrt{1-\xi^2}$ Damped natural frequency

The maximum steady-state response due to mass unbalance occurs at

$\Omega_{peak} = \frac{\omega_n}{\sqrt{1-2\xi^2}}$ with amplitude = $\frac{e}{2\xi\sqrt{1-\xi^2}}$

The numerical results are summarized below:

Numerical results	X direction	Y direction
Undamped Natural Frequency (R/S)	10	20
Undamped Natural Frequency (RPM)	95	191
For *C*=4		
Damping Factor (Zeta)	0.2	0.10
Damped Natural Frequency (RPM)	94	190
Max. Amplitude at Speed (RPM)	100	193
Max. Amplitude	2.552	5.025

The whirl speed map for this simple system was shown in Figure 3.3-1. The steady-state unbalance response for speeds from 0 to 300 rpm with an increment of 1 rpm was analyzed using ***DyRoBeS***. The Bode Plot for the x and y displacements are presented in Figure 3.4-3.

As expected, there is a peak response at each direction due to the bearing asymmetry. The maximum amplitudes and speeds calculated using ***DyRoBeS***, are in agreement with the analytical solutions. The *y* displacement phase angle (ϕ_y) equals the *x* displacement phase angle (ϕ_x) at the rotor speed of 98 rpm that is greater than the first undamped natural frequency of 95 rpm, and at the rotor speed of 186 rpm that is less than the second undamped natural frequency of 191 rpm. That is:

$\pi > (\phi_y - \phi_x) > 0$ when $\Omega < 98$ rpm and $\Omega > 186$ rpm

$\pi > (\phi_x - \phi_y) > 0$ when $98\text{ rpm} < \Omega < 186$ rpm

$\phi_x = \phi_y$ when $\Omega = 98$ rpm and $\Omega = 186$ rpm

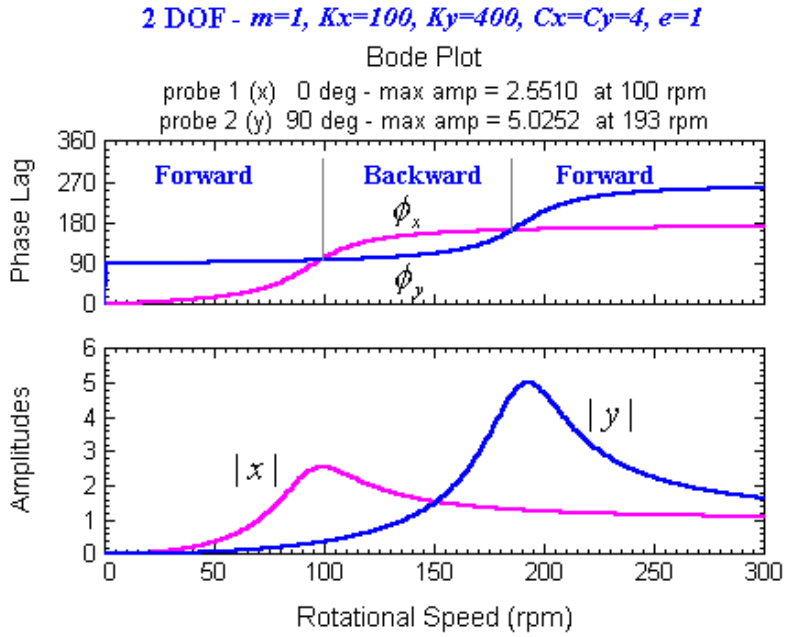

Figure 3.4-3 Bode plot for 2DOF system with unbalance

It indicates that the rotor whirls in forward precession when the rotor speed is below 98 rpm and oscillates along a straight line at 98 rpm. Then it reverses the direction of precession and becomes a backward precession until the rotor speed reaches 186 rpm, where the rotor oscillates along a straight line again. When the rotor speed is above 186 rpm, the direction of precession is reversed from a backward to a forward precession. This phenomenon can be easily observed from the phase angle data shown in the Bode plot and also from the major and minor axes of the elliptical orbit plot, as shown in Figure 3.4-4. The negative semi-minor axis indicates the backward precession. The orbit changes its direction of precession by going through the straight-line motion.

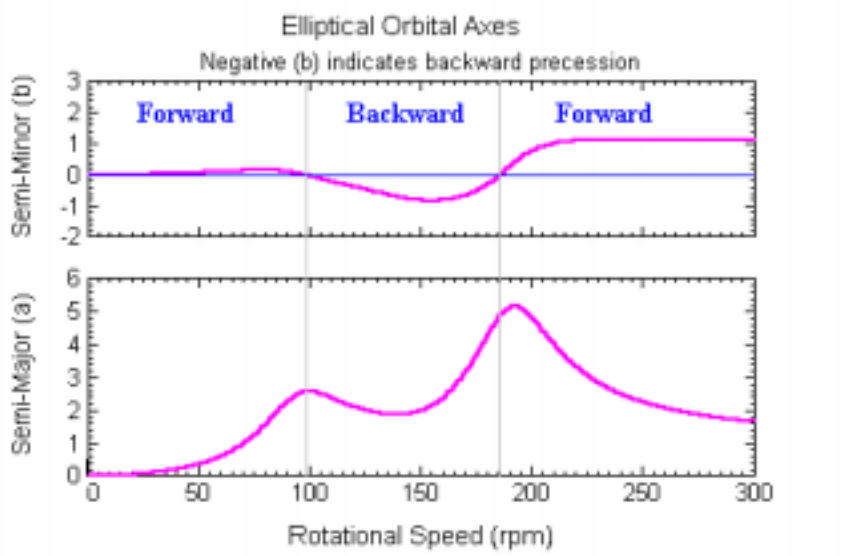

Figure 3.4-4 Elliptical orbital axes

Several orbits at different rotor speeds are shown in Figure 3.4-5. For systems with damping, the straight-line motions will not be aligned in the X or Y axes, due to the damping effect.

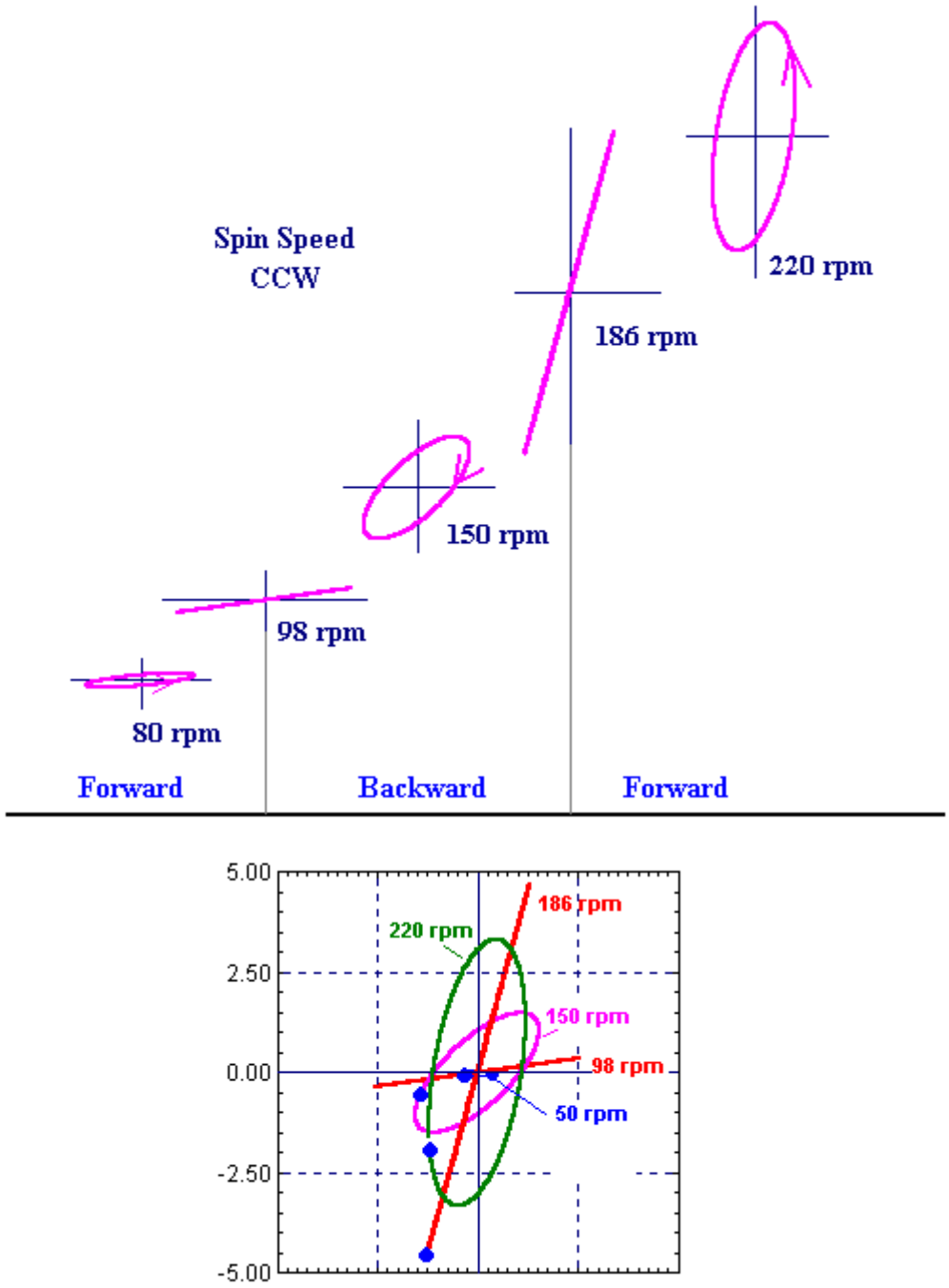

Figure 3.4-5 Steady state rotor orbits at different rotor speeds

This phenomenon can also easily be observed by utilizing the *Displacement Orbit Animation* feature provided by ***DyRoBeS***. Readers are encouraged to run the *Startup/Shutdown Animation*, to visualize the orbit changing sizes and directions as the rotor speed increases or decreases, as illustrated in Figure 3.4-6.

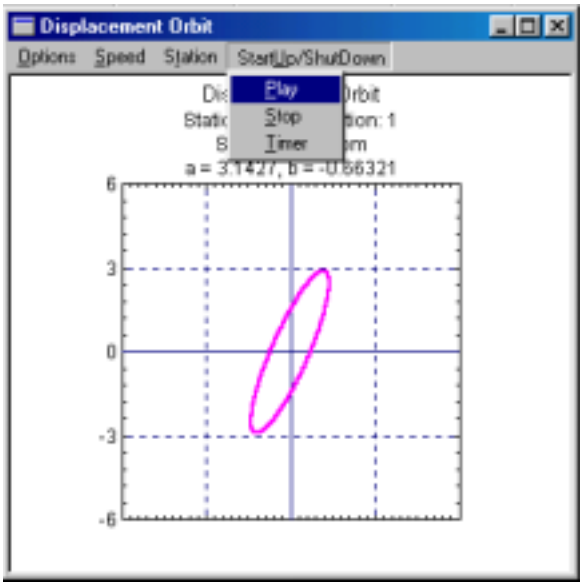

Figure 3.4-6 Animation for the orbits startup and shutdown

Typically, the vibration probes (displacement pick-up) are not in the X and Y directions. The Bode plot at the probes locations can be quite different from the x and y displacements as illustrated in Figure 3.4-7. Figure 3.4-8 is the Bode plot for probes located at 45 and 135 degrees, measured from the X axis, respectively.

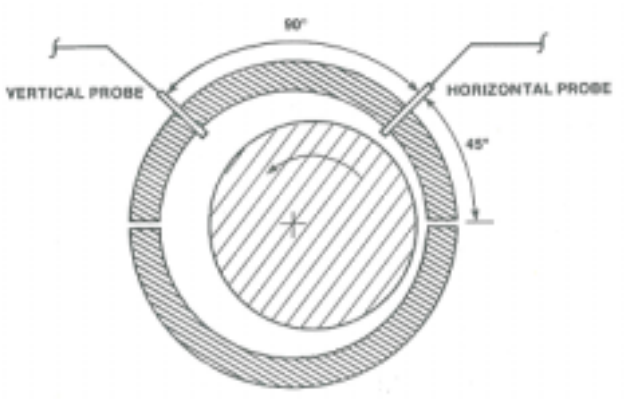

Figure 3.4-7 Two vibration probes

Unlike the Bode plot for the *x* and *y* displacement in Figure 3.4-3, there are two peak responses at each probe in Figure 3.4-8. Each peak corresponds to a resonance condition: one for each natural frequency. One can still identify the forward/backward precessions and straight-line motion by the difference in the phase angles.

Forward precession: $\pi > (\phi_y - \phi_x) > 0$, or $3\pi > (\phi_y - \phi_x) > 2\pi$, and so on.

Backward precession: $2\pi > (\phi_y - \phi_x) > \pi$, or $0 > (\phi_y - \phi_x) > -\pi$, and so on.

Straight-Line Motion: $(\phi_y - \phi_x) = 0, \pi, 2\pi, 3\pi$, and so on.

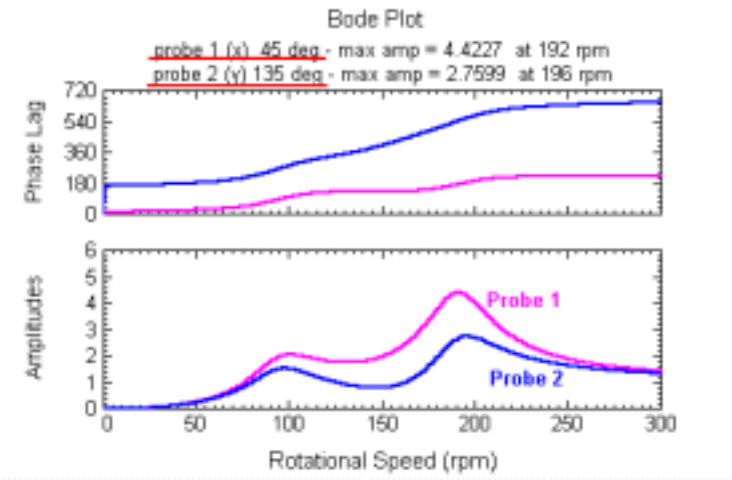

Figure 3.4-8 Bode plot for two probes

It is common in many Industry Standards that utilize the peak amplitude measurements at the vibration probes, to locate the critical speeds instead of using the natural frequencies to define the critical speeds. The above figure shows that for different probe angles, the result can be significantly different. Caution must be taken when utilizing the response measurements to define critical speeds.

It is also noted that for this damped system, the range between two transition speeds where the straight-line motion occurred, is smaller than those in the undamped system. It indicates that the speed range for the backward precession gets smaller as damping increases. In this example, when C=Cx=Cy=10 ($\xi_x = 0.5$ and $\xi_y = 0.25$), there is only one speed (135 rpm), which has a straight-line motion. When C>10, there is no straight-line motion and backward precession does not exist. The major and minor axes of the elliptical orbits for various damping are plotted below:

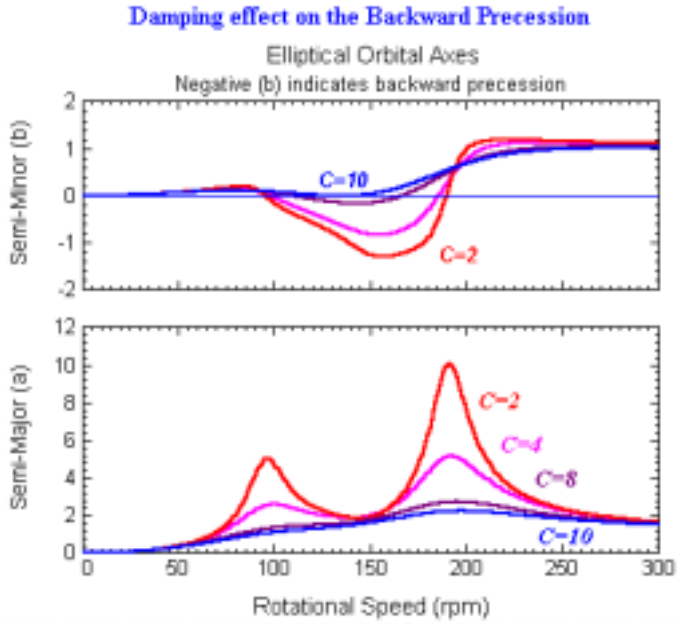

Figure 3.4-9 Elliptical orbital axes for various damping levels

Since this is a simple 2DOF model, the speeds for the straight-line motion can be obtained mathematically from the equations derived before. For the orbit to be a straight-line motion, we have:

$$b = 0, \qquad \text{or} \qquad \phi_x = \phi_y \tag{3.4-26}$$

By substitution phase equations (3.4-4) and (3.4-6) into Equation (3.4-26), yields

$$\tan^{-1}\left(\frac{C_x\Omega}{K_x - M\Omega^2}\right) = \tan^{-1}\left(\frac{C_y\Omega}{K_y - M\Omega^2}\right) + \frac{\pi}{2} \tag{3.4-27}$$

By using the following relationships:

$$\tan^{-1}\alpha = \frac{\pi}{2} - \tan^{-1}\frac{1}{\alpha} \tag{3.4-28}$$

and

$$\tan^{-1}\alpha = -\tan(-\alpha) \tag{3.4-29}$$

We have

$$M^2\Omega^4 + \left(C_xC_y - M\left(K_x + K_y\right)\right)\Omega^2 + K_xK_y = 0 \tag{3.4-30}$$

This draws the same conclusion as presented before, by using the semi-minor axis magnitude equation or the rate of precession. For a given simple Laval-Jeffcott rotor system as presented in this example, the above equation can be used to determine the speeds where the straight-line motion occurs. The speeds where straight-line motions occurred, by using the above equation, can be graphed versus damping (*C=Cx=Cy*) in Figure 3.4-10.

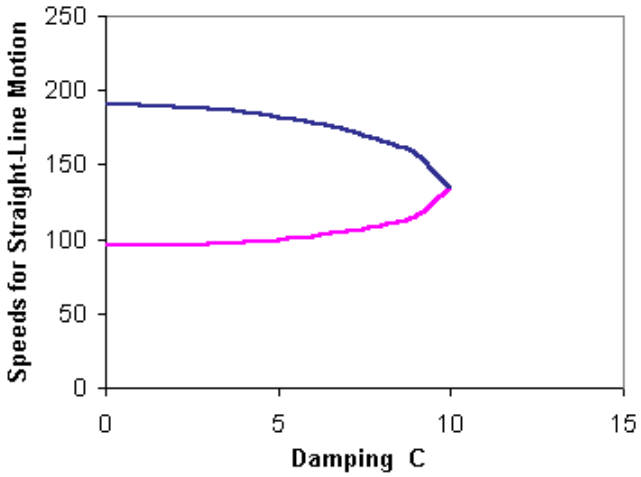

Figure 3.4-10 Speeds for straight-line motion vs. damping

However, for the above equation to have real roots, the following equation must be satisfied:

$$\left(C_x C_y - M\left(K_x + K_y\right)\right)^2 - 4M^2 K_x K_y \geq 0 \tag{3.4-31}$$

The equal sign can also be used to determine if the change in the direction of precession exists or not. The results are identical to those obtained from the steady-state response analysis, by varying the damping for every analysis as shown in Figure 3.4-9. It is evident from Eq. (3.4-31) that for the undamped system, the two straight-line motions occur at the two undamped natural frequencies (95, 191 rpm). As the damping increases, these two speeds approach each other with different approaching rates. When damping reaches a certain value (*C*=10 in this case), the backward precession does not exist anymore, thus there will be no straight-line motion.

The amount of damping required to eliminate the backward precession is also dependent upon the bearing asymmetry. Figure 3.4-11 shows the damping required to eliminate the backward precession for a range of bearing asymmetry.

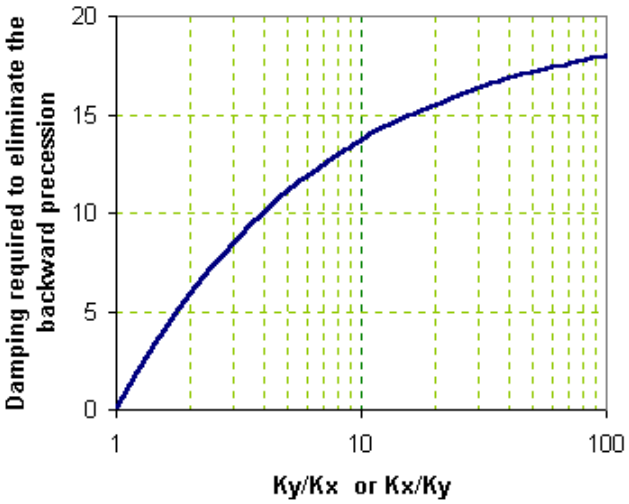

Figure 3.4-11 Damping required to eliminate the backward precession

It shows that for an isotropic system (*Ky/Kx*=1), the displacement orbit is forward circular and no straight-line motion exists. As the bearing asymmetry increases, more damping is required to eliminate the backward precession.

3.5 Steady State Response to Shaft Bow

The residual shaft bow may be present in the rotor-bearing systems due to many various reasons, including assembly tolerances and uneven thermal distribution. When the residual shaft bow exists in a rotor system, a constant magnitude rotating force synchronized with the shaft spin speed acts on the rotor system. The excitation force caused by the residual shaft bow is of the form:

$$F = K_s q_b \tag{3.5-1}$$

where K_s is the shaft bending stiffness and q_b is the amount of shaft initial displacements in fixed reference frame, due to residual shaft bow. The shaft bow rotates with the rotating reference and is specified in the rotating reference frame. By utilizing the coordinate transformation between fixed and rotating reference frames, presented in Chapter 2, the synchronous excitation force due to the residual shaft bow in the fixed reference frame becomes:

$$\begin{Bmatrix} F_x \\ F_y \end{Bmatrix} = K_s \left(\begin{Bmatrix} x' \\ y' \end{Bmatrix} \cos \Omega t + \begin{Bmatrix} -y' \\ x' \end{Bmatrix} \sin \Omega t \right) \tag{3.5-2}$$

The synchronous excitation force due to residual shaft bow is similar to the synchronous excitation due to mass unbalance. However, the excitation amplitude of a shaft bow is a constant, while the excitation amplitude of an unbalance is a function of square of spin speed.

Example 3.2: Laval-Jeffcott Rotor– Residual Shaft Bow and Unbalance Response

A Laval-Jeffcott rotor system supported by rigid bearings is presented in this example to demonstrate the steady-state response due to shaft bow, mass imbalance, and their combined effects. As shown in the following Figure 3.5-1, a rigid disk is located at the midspan of a flexible shaft with residual shaft bow. Since only the fundamental translational motion is considered, the rigid disk has a mass of 4 Lbm (0.01036 Lbf-s^2/in) and zero mass moment of inertia (I_d=I_p=0). The flexible shaft with elastic modulus of 3.0E07 psi has a length of 12 inches and a diameter of 0.275 inches. The shaft mass is negligible in this case, otherwise, the shaft modal mass ($0.4857\rho AL$) needs to be added into the disk to form an effective (modal) mass for this translational motion, as demonstrated in Chapter 1. A linear isotropic viscous damping with a value of C=0.3114 Lbf-s/in, is applied at the disk location. For demonstrative purposes, the pertinent parameters for this Laval-Jeffcott rotor are summarized below:

L = 12.0 in (total length)
D = 0.275 in (shaft diameter)
E = 3.0E07 psi (Young's modulus)
M = 4.0 Lbm (0.01036 Lbf-s^2/in) (disk mass)
C = 0.3114 Lbf-s/in (viscous damping at disk)
e = 0.001 in (mass eccentricity)
q_b= 0.001 in (shaft bow at disk)

The translational stiffness at the midspan of the shaft due to bending is:

$$K = \frac{48EI}{L^3} = 233.95 \text{ Lbf/in} \quad \text{where} \quad I = \frac{\pi D^4}{64}$$

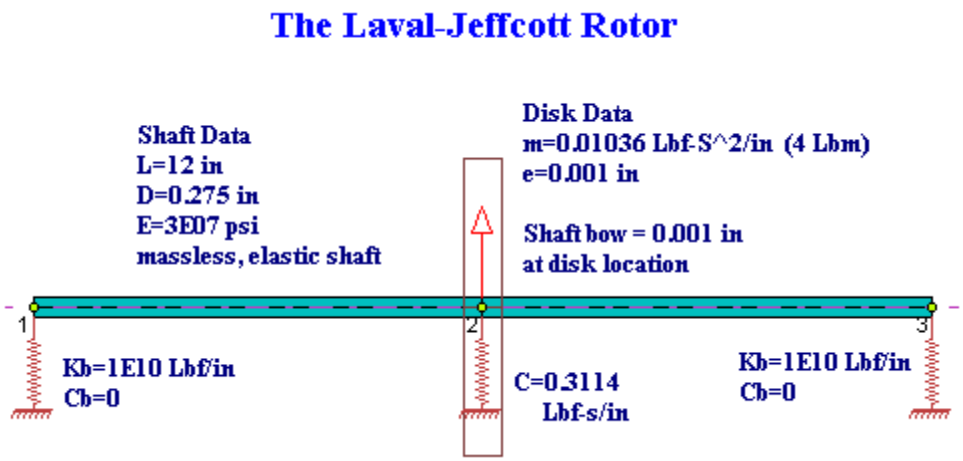

Figure 3.5-1 The Laval-Jeffcott rotor

This simple 2DOF system can be modeled by using geometric constraints, that is, constrain all the degrees-of-freedom at stations 1 and 3, and rotational degrees-of-freedom at station 2, as demonstrated in the earlier examples. However, in this example a bearing stiffness of 1E10 Lbf/in is applied at both ends, instead of constraints as used in earlier examples. This bearing stiffness is much larger than the shaft bending stiffness. Therefore, they act like rigid bearings. Without loss of generality, the residual bow is assumed to be:

$$x' = q_b, \quad \text{and} \quad y' = 0$$

The above assumption is similar to assuming the phase angle of unbalance eccentricity be zero in the unbalance response analysis, which was presented in the previous sections. However, the phase angle of the unbalance force in this example is a parameter that will be studied.